



## RESEARCH LETTER

10.1002/2014GL061421

## Key Points:

- Solar-driven ionospheric potential changes affect pressure in polar troposphere
- Location and timescale suggest involvement of cloud microphysics
- Fast tropospheric response contrasts to UV and particle precipitation mechanisms

## Correspondence to:

M. M. Lam,  
maimailam7@gmail.com

## Citation:

Lam, M. M., G. Chisham, and M. P. Freeman (2014), Solar wind-driven geopotential height anomalies originate in the Antarctic lower troposphere, *Geophys. Res. Lett.*, *41*, 6509–6514, doi:10.1002/2014GL061421.

Received 1 AUG 2014

Accepted 27 AUG 2014

Accepted article online 28 AUG 2014

Published online 22 SEP 2014

## Solar wind-driven geopotential height anomalies originate in the Antarctic lower troposphere

Mai Mai Lam<sup>1</sup>, Gareth Chisham<sup>1</sup>, and Mervyn P. Freeman<sup>1</sup>

<sup>1</sup>British Antarctic Survey, Natural Environment Research Council, Cambridge, UK

**Abstract** We use National Centers for Environmental Prediction/National Center for Atmospheric Research reanalysis data to estimate the altitude and time lag dependence of the correlation between the interplanetary magnetic field component,  $B_y$ , and the geopotential height anomaly above Antarctica. The correlation is most statistically significant within the troposphere. The peak in the correlation occurs at greater time lags at the tropopause (~6–8 days) and in the midtroposphere (~4 days) than in the lower troposphere (~1 day). This supports a mechanism involving the action of the global atmospheric electric circuit, modified by variations in the solar wind, on lower tropospheric clouds. The increase in time lag with increasing altitude is consistent with the upward propagation by conventional atmospheric processes of the solar wind-induced variability in the lower troposphere. This is in contrast to the downward propagation of atmospheric effects to the lower troposphere from the stratosphere due to solar variability-driven mechanisms involving ultraviolet radiation or energetic particle precipitation.

### 1. Introduction

Meteorological effects resulting from fluctuations in the solar wind are presently poorly represented in atmospheric models. Indeed, the role of the Sun is one of the largest unknowns in the climate system [Le Treut *et al.*, 2007]. A number of large-scale atmospheric dynamic changes are known to occur, on a day-to-day timescale, in response to changes in the downward current density of the global atmospheric electric circuit (GEC) [Tinsley, 2008]. One well-established example of this is the Mansurov effect. This is a response in the surface atmospheric pressure anomaly (with respect to the seasonal average) in the polar regions to changes in the dawn-dusk component of the interplanetary magnetic field (IMF),  $B_y$  [Mansurov *et al.*, 1974; Tinsley and Heelis, 1993; Burns *et al.*, 2007, 2008; Lam *et al.*, 2013]. Making use of the consistently high-quality IMF data that are available from 1995 onward, the amplitude and statistical significance of the Mansurov effect have been found to be most pronounced in the Antarctic region. Specifically, the variation in the daily average of IMF  $B_y$  across a range of ~8 nT has been associated with changes in the high-latitude surface atmospheric pressure anomaly of ~1–2 hPa [Burns *et al.*, 2008; Lam *et al.*, 2013]. For the interval 1995–2005, the effect is found to be statistically significant in Antarctica but not in the Arctic, where it is only significant for the period 1999–2002 [Burns *et al.*, 2008].

There is evidence to suggest that the Mansurov effect is a manifestation of Sun-weather coupling that occurs via the GEC [see Tinsley, 2008, and references therein]. First, as IMF  $B_y$  changes from large and negative to large and positive, there is a correspondence between the sign and location of the change in surface pressure anomaly and the sign and location of the change in the ionospheric electric potential [e.g., Lam *et al.*, 2013, Figure 2]. Second, the time between changes in IMF  $B_y$  and changes in the surface pressure anomaly is short (within 3 days) [Burns *et al.*, 2007, 2008]. Third, the sensitivity of high-latitude surface pressure anomaly variations to the GEC-driven changes in the surface vertical electric field is similar, whether the source is the external IMF  $B_y$  generator or the internal meteorological generator driven by thunderstorms and electrified clouds [Burns *et al.*, 2008].

Figure 1 is a schematic representation of the postulated processes through which the GEC affects polar weather to produce the Mansurov effect. The observed correlation between IMF  $B_y$  and surface pressure anomaly is represented by (A), while the proposed physical mechanism acts via paths (B)–(E). Path (B) represents the continual interaction of the solar wind with the Earth's magnetosphere via magnetic reconnection, a fundamental physical process responsible for much of the transfer of mass, momentum, and energy from the solar wind into the Earth's magnetosphere and ionosphere. Reconnection drives the transport of plasma through the magnetosphere which results in variations in the electric field in the high-latitude polar cap

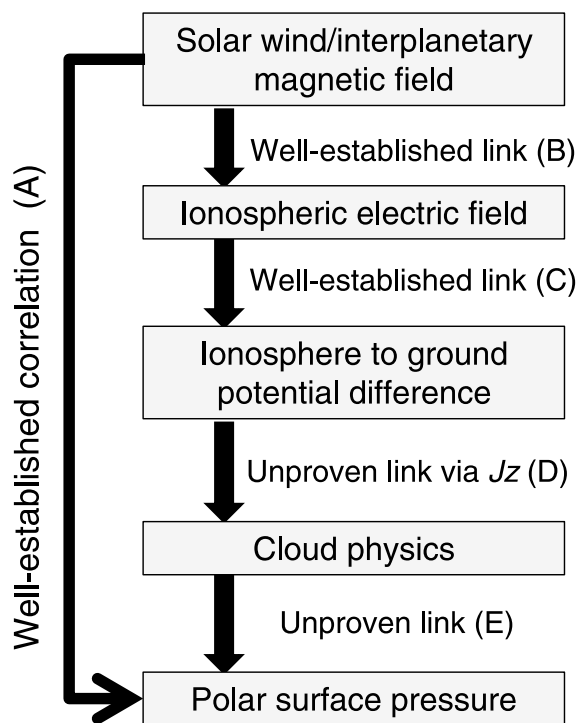


**Figure 1.** A schematic representation of how the proposed global atmospheric electric circuit mechanism produces the correlation between fluctuations in the dawn-dusk component of the interplanetary magnetic field (IMF),  $B_y$ , and surface atmospheric pressure. The observed IMF  $B_y$  surface pressure correlation, known as the Mansurov effect, is represented by (A), while the proposed physical mechanism acts via paths (B)–(E).

and duskside of the polar cap. This means that at a given geographical location, this influence largely cancels out over a day [Burns *et al.*, 2007]. No substantial relationship is found between the surface pressure anomaly and the daily average of IMF  $B_z$  at Antarctic station Vostok located close to the magnetic pole ( $84^\circ\text{S}$ ) [Burns *et al.*, 2007]. This lack of correlation between IMF  $B_z$  and surface pressure is consistent with a mechanism driven by the *day-to-day* variability in the daily average ionosphere-to-ground potential difference.

Path (D) in Figure 1 represents postulated processes in which variability in microphysical (and thereby macrophysical) cloud properties is driven by variability in the GEC vertical current density  $J_z$  [e.g., Tinsley, 2008, Rycroft *et al.*, 2012]. For instance, layer cloud edges are charged by the vertical current flow in the GEC [Nicoll and Harrison, 2009, 2010]. The resulting generation of space charge on cloud edges [Zhou and Tinsley, 2007] leads to the transfer of charge to cloud droplets and aerosol particles in these regions, which theoretical modeling studies show can influence several cloud microphysical processes [see Rycroft *et al.*, 2012, and references therein]. Any processes (solar driven or otherwise) that modify either the ionosphere-to-ground potential difference or under some circumstances the atmospheric conductivity within the GEC [Tinsley *et al.*, 2012], vary  $J_z$ . Varying  $J_z$ , therefore, may lead to variation in cloud microphysical properties, with possible consequences for atmospheric and climate processes ((E) in Figure 1).

Our aim in this paper is to examine whether the Mansurov effect, which until now has been reported only at the Earth's surface, exists farther up in the atmospheric column. In doing so, we aim to shed light on the origins of the surface correlation. In particular, we investigate the theory that the lower atmosphere is influenced by the action of the GEC on cloud physics by examining the altitude-time lag and the latitude-time lag signatures of the correlation. In section 2, we present the data sets and methodology; the results are given in section 3, and a discussion with conclusions is given in section 4.

ionosphere that depend on the IMF magnitude and direction [e.g., Cowley and Lockwood, 1992]. The dependence of the ionospheric electric field on the solar wind and the IMF is well established [e.g., Pettigrew *et al.*, 2010; Weimer, 2005].

The world's thunderstorms and electrified clouds maintain a vertical electrical potential drop of about 250 kV between the ground and the ionosphere [Williams, 2005]. The solar wind-driven changes in the horizontal component of the ionospheric electric field result in a spatial and IMF  $B_y$ -dependent *daily average* perturbation of between  $-30$  and  $30$  kV to this potential drop at high geomagnetic latitudes ( $>75^\circ\text{S}$ ) [Burns *et al.*, 2007]. In Figure 1, the link (C) represents the simple downward electrostatic mapping of ionospheric potential changes to surface vertical electric field changes. These are associated with changes in the downward current density  $J_z$ . In contrast, the daily average contribution associated with the north-south component of the IMF,  $B_z$ , is small at high geomagnetic latitudes because, although  $B_z$  has a strong influence on the electric potential perturbation, it is equal and approximately opposite on the dawnside

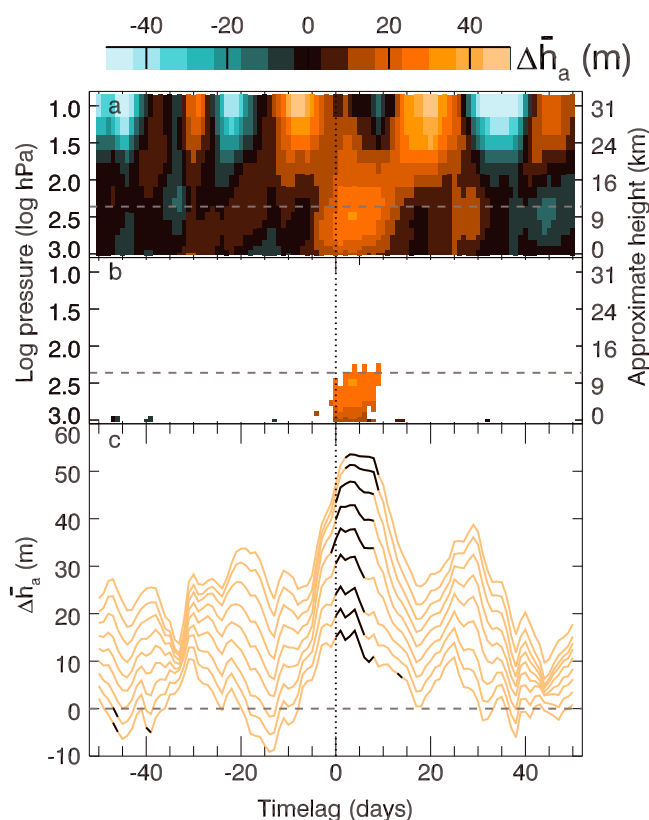


**Figure 2.** The Mansurov effect is confined to the troposphere and the base of the stratosphere in Antarctica. (a)  $\Delta\bar{h}_a(\tau, p)$ , the difference in the 1999–2002 Antarctic field mean in geopotential height anomaly between IMF  $B_y \geq 3$  nT and IMF  $B_y \leq -3$  nT states (equation (1)). IMF  $B_y$  acts as a proxy for the horizontal component of the ionospheric electric field. A minimum (winter) pressure level for the Antarctic tropopause of 230 hPa is marked by the horizontal grey dashed line. A maximum (summer) pressure level for the Antarctic tropopause is 330 hPa [Zangl and Hoinka, 2001]; (b) as for Figure 2a but masked at the 1% field significance level.  $\Delta\bar{h}_a$  is of statistically significant amplitude within the troposphere and the base of the stratosphere at the 1% field significance levels. At any given pressure level, the peak correlation occurs for positive time lag consistent with solar wind-driven ionospheric electric field fluctuations leading the atmospheric response; (c)  $\Delta\bar{h}_a$  is plotted at different pressure levels with a 3 m offset between each decreasing pressure level to help with visualization. Statistically significant values at the 1% level are plotted in black, and values of less statistical significance are plotted in orange. Starting with the line plotted at the bottom of the panel, the levels plotted are 1000, 925, 850, 700, 600, 500, 400, 300, and 250 hPa. The temporally broad peak shifts to increased time lags with increasing altitude, suggestive of an upward propagation of the Mansurov effect from the lower to upper troposphere.

$\bar{h}_{z+}(\lambda, \tau, p)$  and  $\bar{h}_{z-}(\lambda, \tau, p)$ , respectively. The geocentric solar magnetospheric (GSM) coordinate system is used for the IMF data, where positive  $B_y$  is aligned from dawn to dusk. The time lag between IMF  $B_y$  and geopotential height is defined so that IMF  $B_y$  leads geopotential height for  $\tau > 0$ . Data are excluded that lie below the Earth's surface, as specified by the NCEP/NCAR topography.

To assess the statistical significance of the correlation between the IMF and the geopotential height anomaly, we conduct a nonparametric Wilcoxon Rank-Sum test (WRST) of the difference in the mean geopotential height anomaly for the two IMF  $B_y$  states. The test outputs a nearly normal test statistic  $Z(\lambda, \phi, \tau, p)$  and the one-tailed probability of obtaining a value of  $Z$  or greater by chance.

## 2. Data Sets and Method

We examine the interval 1999–2002 when statistically significant correlations between daily averaged IMF  $B_y$  and 12 UT surface pressure anomaly were seen in both the Arctic and in Antarctica [Burns et al., 2008; Lam et al., 2013]. We extend our zero time lag ( $\tau = 0$ ) surface pressure study [Lam et al., 2013] upward to a height of about 31 km, using a similar methodology to examine the correlation between the daily average of IMF  $B_y$  and the Antarctic atmospheric geopotential height anomaly. To obtain this anomaly, the seasonal cycle was removed from 12 UT National Centers for Environmental Prediction/ National Center for Atmospheric Research (NCEP/NCAR) geopotential height data [Kalnay et al., 1996] for the 17 available pressure levels. These cover the pressure range 10–1000 hPa corresponding to an altitude range between about 31 km and close to sea level. The seasonal cycle is approximated by the mean 12 UT value for each “day of year” on the model latitude  $\lambda$ , longitude  $\phi$ , and pressure level  $p$  grid, using 1948–2011 data.

We determined the 4 year mean of the geopotential height anomaly for two distinct states of the solar wind magnetic field: high positive IMF  $B_y$  ( $\geq 3$  nT) and high negative  $B_y$  ( $\leq -3$  nT). This was done on a latitude, longitude, daily time lag, and pressure level grid. We denote these quantities by  $\bar{h}_+(\lambda, \phi, \tau, p)$  and  $\bar{h}_-(\lambda, \phi, \tau, p)$ . The corresponding zonal means are denoted by

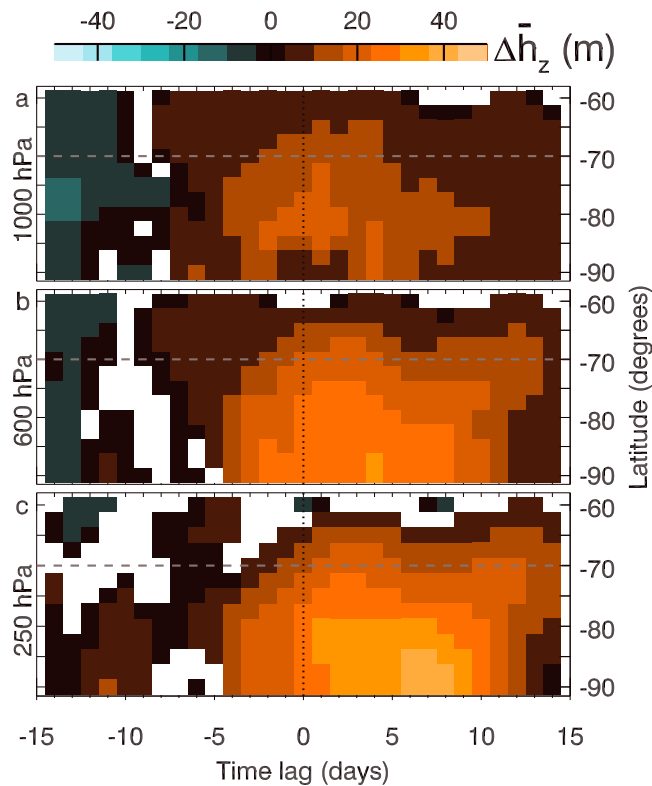


**Figure 3.** Evidence to support the hypothesis that the Mansurov effect originates in the lower troposphere (~1000 hPa), propagates through the midtroposphere (e.g., 600 hPa) to the tropopause region (~250 hPa).  $\Delta\bar{h}_z(\lambda, \tau, p)$ , the difference between the 1999 and 2002 zonal mean of the geopotential height anomaly for  $\text{IMF } B_y \geq 3 \text{ nT}$  and  $\text{IMF } B_y \leq -3 \text{ nT}$  (equation (2)) at (a) 1000 hPa, (b) 600 hPa, and (c) 250 hPa as a function of latitude and time lag between the solar wind and geopotential height data. The peak amplitude occurs for positive time lag, consistent with the solar wind leading the atmospheric response and at increasing time lag as the pressure level decreases and altitude increases. We have used the one-tailed probability from a Wilcoxon Rank Sum Test (WRST) between  $\bar{h}_{z+}(\lambda, \tau, p)$  and  $\bar{h}_{z-}(\lambda, \tau, p)$  to mask the results at the 1% level. The horizontal dashed line marks 70°S. The area poleward of this latitude is used to derive the field mean values plotted in Figure 2.

a significant value could occur by chance with a probability above the 1% level (Figure 2b). The difference between  $\bar{h}_{a+}$  and  $\bar{h}_{a-}$  is highly statistically significant (the probability is below the 1% level) for time lags between 0 and 10 days in the troposphere and at the base of the stratosphere. The results presented in Figures 2a and 2b give a high degree of confidence in a response, on a timescale of days, of the pressure in the troposphere and the base of the stratosphere to changes in the horizontal component of the ionospheric electric field. The temporally broad peak of the field mean  $\Delta\bar{h}_a$  shifts to later time lags as the altitude in the troposphere increases (Figure 2c), which is suggestive of an upward propagation of the Mansurov effect which originates in the lower troposphere. It is in part the high degree of temporal autocorrelation in the IMF that gives rise to the broad 10–15 day width for the peak in the correlation. In addition, there is evidence for an accumulation of the meteorological effect of the GEC over about 3 days when IMF  $B_y$  maintains its value for more than a few days [Burns et al., 2007, 2008].

**3.2. Latitude-Time Lag Signal at Different Altitudes**

We next examine the latitude-time lag signature of the Mansurov effect at different altitudes using the zonal mean

$$\Delta\bar{h}_z(\lambda, \tau, p) = \bar{h}_{z+}(\lambda, \tau, p) - \bar{h}_{z-}(\lambda, \tau, p) \tag{2}$$

**3. Results**

**3.1. Altitude Range of the Mansurov Effect**

Globally, the highest statistical significance for the correlation between IMF  $B_y$  and the regional-mean surface pressure anomaly has been found for the region poleward of 70°S [see Lam et al., 2013, Table 1]. It is in this region, therefore, that we conduct the altitude-time lag study. For a given pressure level, atmospheric variables such as the geopotential height have a high degree of spatial autocorrelation. This results in a fraction of local null hypotheses such as “there is no difference between  $\bar{h}_+(\lambda, \phi, \tau, p)$  and  $\bar{h}_-(\lambda, \phi, \tau, p)$ ” being rejected by significance tests that should not be rejected. When evaluating statistical significance values, we correct for this false discovery rate by finding the field significance [Wilks, 2006]  $\eta_a(\tau, p)$  for the region defined by  $\lambda \geq 70^\circ\text{S}$  at each time lag and pressure level. The mean values of  $\bar{h}_+(\lambda, \phi, \tau, p)$  and  $\bar{h}_-(\lambda, \phi, \tau, p)$  for this geographical region are  $\bar{h}_{a+}(\tau, p)$  and  $\bar{h}_{a-}(\tau, p)$  where “a” denotes “Antarctic.” The difference in the Antarctic field mean values for high-positive and high-negative  $B_y$

$$\Delta\bar{h}_a(\tau, p) = \bar{h}_{a+}(\tau, p) - \bar{h}_{a-}(\tau, p) \tag{1}$$

is plotted in Figure 2a. The field statistical significance  $\eta_a(\tau, p)$  relating to the difference  $\Delta\bar{h}_a(\tau, p)$  is used to mask out values of  $\Delta\bar{h}_a(\tau, p)$  where

At 1000 hPa, corresponding to an altitude of  $\sim 0.1$  km, the near-surface Mansurov effect is mostly confined to latitudes poleward of  $70^\circ\text{S}$  and persists about 10–15 days (Figure 3a). The amplitude of  $\Delta\bar{h}_z(\lambda, \tau, p)$  has a peak, significant at the 1% level, when the IMF leads the reanalysis data set by 1 day which spans  $\sim 72.5^\circ\text{--}87.5^\circ\text{S}$ . Temporally, the peak at  $\sim 82.5^\circ\text{S}$  spans time lags of  $-2$  to 2 days. A second peak exists at a time lag of 4 days spanning  $\sim 82.5\text{--}90^\circ\text{S}$ . The results at 1000 hPa are consistent with results from previous studies using station data at the Earth's surface [Burns *et al.*, 2007, 2008] which find that the Mansurov effect peaks poleward of  $80^\circ\text{S}$  magnetic latitude, when the IMF leads the pressure by  $0\pm 2$  days and with the effect persisting over a period of about 10 days.

At 600 hPa (Figure 3b), corresponding to an altitude of  $\sim 4.2$  km in the middle troposphere, the peak in the latitude-time lag signature is located close to the geographic pole when IMF  $B_y$  leads geopotential height by 4 days. An even longer time lag, of around 6–8 days, is observed for the peak of the correlation between  $B_y$  and the geopotential height anomaly at 250 hPa ( $\sim 10.4$  km) near the winter tropopause as shown in Figure 3c. At this altitude, the peak is once again located close to the pole, between  $85$  and  $90^\circ\text{S}$ . The increase in the time lag of the peak in  $\Delta\bar{h}_z(\lambda, \tau, p)$  with increasing altitude is suggestive of an upward propagation of the solar wind-induced variability in the lower troposphere.

#### 4. Discussion and Conclusions

The use of reanalysis data over the last decade to measure and characterize the relationship between solar activity and the atmosphere [e.g., Gray *et al.*, 2010; Veretenenko and Thejll, 2005; Seppälä *et al.*, 2009, and references therein] has significantly improved our understanding of the effects of solar variability on weather and climate. Like all the reanalysis data sets, the NCEP/NCAR reanalysis data set is generated by combining meteorological observations and meteorological numerical weather prediction models so that the observational values are preserved where they are present and physically consistent values are created by a model to fill the gaps in the observations. Since this study is performed in the modern era, the reanalysis incorporates regularly collected weather balloon data (usually daily) and satellite data. The main limitation here is the relatively spatially sparse data collection in Antarctica. There are about 20 stations which collect data once daily for the interval in question at standard meteorological pressure levels up to about 30 hPa ( $\sim 23.8$  km). However, we do not investigate far above the altitude where measurements exist.

To date, three major mechanisms have been proposed by which solar variability affects weather and climate: (1) the effect of solar UV variability on stratospheric ozone chemistry and hence on the atmospheric radiation balance [e.g., Gray *et al.*, 2010; Ineson *et al.*, 2011; Ermolli *et al.*, 2013], (2) the effect of energetic particle precipitation from the space environment, modulated by solar variability, on stratospheric ozone chemistry and hence on the atmospheric radiation balance [e.g., Rozanov *et al.*, 2012; Seppälä and Clilverd, 2014], and (3) the effect of variations in the GEC, modulated by variations in the solar wind driven by solar variability, on cloud properties and consequently on meteorology [e.g., Tinsley, 2008; Rycroft *et al.*, 2012]. The third of these mechanisms, the “GEC mechanism,” is explored in this paper. It remains the least well understood and the most underexplored. A complete understanding of this mechanism is necessary if the effects of solar variability are to be fully integrated into weather and climate models. It should be noted that the meteorological effects of this high-latitude solar wind-driven GEC effect extend beyond the polar regions to the midlatitudes [Lam *et al.*, 2013] and therefore may contribute to solar-meteorological correlations which have been observed there [Tinsley, 2008].

In conclusion, we have shown the presence of a statistically significant correlation between the interplanetary magnetic field and geopotential height within the troposphere over Antarctica up to the region of the winter tropopause. The timescale of this phenomenon is of the order of days. This is consistent with the action of the GEC mechanism, driven by solar wind-driven variations in the ionosphere-to-ground electric potential difference, on lower tropospheric clouds. The relatively fast timescale and the apparent upward propagation of this solar wind-induced effect are in contrast to the downward propagation, on a timescale of months, of meteorological effects to the lower troposphere from the stratosphere due to other mechanisms associated with solar variability, involving ultraviolet radiation or energetic particle precipitation.

### Acknowledgments

NCEP/NCAR reanalysis data were provided by the NOAA/OAR/ ESRL PSD, Boulder, Colorado, USA, from their website <http://www.esrl.noaa.gov/psd/>. The OMNI data were obtained from the GSFC/SPDF OMNIWeb interface at <http://omniweb.gsfc.nasa.gov>. We thank the COST Action ES1005 TOSCA for financial support to attend TOSCA workshops which stimulated useful discussions contributing to the development of this work. The authors gratefully acknowledge support by the UK Natural Environment Research Council (NERC) grant NE/I024852/1.

The Editor thanks Michael Rycroft and an anonymous reviewer for their assistance in evaluating this paper.

### References

- Burns, G. B., B. A. Tinsley, A. V. Frank-Kamenetsky, and E. A. Bering (2007), Interplanetary magnetic field and atmospheric electric circuit influences on ground-level pressure at Vostok, *J. Geophys. Res.*, *112*, D04103, doi:10.1029/2006JD007246.
- Burns, G. B., B. A. Tinsley, W. J. R. French, O. A. Troshichev, and A. V. Frank-Kamenetsky (2008), Atmospheric circuit influences on ground-level pressure in the Antarctic and Arctic, *J. Geophys. Res.*, *113*, D15112, doi:10.1029/2007JD009618.
- Cowley, S. W. H., and M. Lockwood (1992), Excitation and decay of solar wind-driven flows in the magnetosphere-ionosphere system, *Ann. Geophys.*, *10*, 103–115.
- Ermolli, I., et al. (2013), Recent variability of the solar spectral irradiance and its impact on climate modelling, *Atmos. Chem. Phys.*, *13*, 3945–3977, doi:10.5194/acp-13-3945-2013.
- Gray, L. J., et al. (2010), Solar influence on climate, *Rev. Geophys.*, *48*, RG4001, doi:10.1029/2009RG000282.
- Ineson, S., A. A. Scaife, J. R. Knight, J. C. Manners, N. J. Dunstone, L. J. Gray, and J. D. Haigh (2011), Solar forcing of winter climate variability in the Northern Hemisphere, *Nat. Geosci.*, *4*, 753–757, doi:10.1038/NNGEO1282.
- Kalnay, E., et al. (1996), The NCEP/NCAR 40-year reanalysis project, *Bull. Am. Meteorol. Soc.*, *77*, 437–471.
- Lam, M. M., G. Chisham, and M. P. Freeman (2013), The interplanetary magnetic field influences mid-latitude surface atmospheric pressure, *Environ. Res. Lett.*, *8*, 045001, doi:10.1088/1748-9326/8/4/045001.
- Le Treut, H., R. Somerville, U. Cubasch, Y. Ding, C. Mauritzen, A. Mokssit, T. Peterson, and M. Prather (2007), Historical overview of climate change, in *Climate Change 2007: The Physical Science Basis. Contribution of Working Group I to the Fourth Assessment Report of the Intergovernmental Panel on Climate Change*, edited by S. Solomon et al., pp. 95–127, Cambridge Univ. Press, Cambridge, U. K.
- Mansurov, S. M., L. G. Mansurova, G. S. Mansurov, V. V. Mikhnevich, and A. M. Visotsky (1974), North-south asymmetry of geomagnetic and tropospheric events, *J. Atmos. Terr. Phys.*, *36*(1), 1957–1962.
- Nicoll, K. A., and R. G. Harrison (2009), Vertical current flow through extensive layer clouds, *J. Atmos. Sol. Terr. Phys.*, *71*, 2040–2046, doi:10.1016/j.jastp.2009.09.011.
- Nicoll, K. A., and R. G. Harrison (2010), Experimental determination of layer cloud edge charging from cosmic ray ionisation, *Geophys. Res. Lett.*, *37*, L13802, doi:10.1029/2010GL043605.
- Pettigrew, E. D., S. G. Shepherd, and J. M. Ruohoniemi (2010), Climatological patterns of high-latitude convection in the Northern and Southern hemispheres: Dipole tilt dependencies and interhemispheric comparisons, *J. Geophys. Res.*, *115*, A07305, doi:10.1029/2009JA014956.
- Rozanov, E., M. Calisto, T. Egorova, T. Peter, and W. Schmutz (2012), Influence of the precipitating energetic particles on atmospheric chemistry and climate, *Surv. Geophys.*, *33*, 483–501, doi:10.1007/s10712-012-9192-0.
- Rycroft, M. J., K. A. Nicoll, K. L. Aplin, and R. G. Harrison (2012), Recent advances in global electric circuit coupling between the space environment and the troposphere, *J. Atmos. Sol. Terr. Phys.*, *90–91*, 198–211, doi:10.1016/j.jastp.2012.03.015.
- Seppälä, A., and M. A. Clilverd (2014), Energetic particle forcing of the Northern Hemisphere winter stratosphere: Comparison to solar irradiance forcing, *Front. Physiol.*, *2*, 25, doi:10.3389/fphys.2014.00025.
- Seppälä, A., C. E. Randall, M. A. Clilverd, E. Rozanov, and C. J. Rodger (2009), Geomagnetic activity and polar surface air temperature variability, *J. Geophys. Res.*, *114*, A10312, doi:10.1029/2008JA014029.
- Tinsley, B. A. (2008), The global atmospheric electric circuit and its effects on cloud microphysics, *Rep. Prog. Phys.*, *71*, 066801, doi:10.1088/0034-4885/71/6/066801.
- Tinsley, B. A., and R. A. Heelis (1993), Correlations of atmospheric dynamics with solar activity: Evidence for a connection via the solar wind, atmospheric electricity, and cloud microphysics, *J. Geophys. Res.*, *98*, 10,375–10,384.
- Tinsley, B. A., L. Zhou, and W. Liu (2012), The role of volcanic aerosols and relativistic electrons in modulating winter storm vorticity, *Adv. Space Res.*, *50*, 819–827, doi:10.1016/j.asr.2011.12.019.
- Veretenenko, S., and P. Thejll (2005), Cyclone regeneration in the North Atlantic intensified by energetic solar proton events, *Atmos. Chem. Phys.*, *35*, 470–475, doi:10.1016/j.asr.2005.01.079.
- Weimer, D. R. (2005), Improved ionospheric electrodynamic models and application to calculating Joule heating rates, *J. Geophys. Res.*, *110*, A05306, doi:10.1029/2004JA010884.
- Wilks, D. S. (2006), On ‘field significance’ and the false discovery rate, *J. Appl. Meteorol. Clim.*, *45*, 1181–1189.
- Williams, E. R. (2005), Lightning and climate: A review, *Atmos. Res.*, *76*, 272–287, doi:10.1016/j.atmosres.2004.11.014.
- Zangl, G., and K. P. Hoinka (2001), The tropopause in the polar regions, *J. Clim.*, *14*, 3117–3139.
- Zhou, L., and B. A. Tinsley (2007), Production of space charge at the boundaries of layer clouds, *J. Geophys. Res.*, *112*, D11203, doi:10.1029/2006JD007998.